Supplementary File

Elucidating lithium ion diffusion kinetics in cation-disordered rocksalt cathodes

*Byungwook Kang[1,+], Jonghun Park[1,+], Byunghoon Kim[1], Sung-O Park[1], Jaekyun Yoo[1], Seungju Yu[1], Hyuk-Joon Kim[1], Jun-Hyuk Song[2] and Kisuk Kang[1,3,4 *]*

[1]Department of Materials Science and Engineering, Institute for Rechargeable Battery Innovations, Research Institute of Advanced Materials, Seoul National University, 1 Gwanak-ro, Gwanak-gu, Seoul 08826, Republic of Korea.

[2]Secondary Battery Materials Lab, POSCO Holdings N.EX.T Hub, Seoul, Republic of Korea

[3]Institute of Engineering Research, College of Engineering, Seoul National University, 1 Gwanak-ro, Gwanak-gu, Seoul 08826, Republic of Korea

[4]Center for Nanoparticle Research, Institute for Basic Science (IBS), Seoul National University, 1 Gwanak-ro, Gwanak-gu, Seoul 08826, Republic of Korea

[+]These authors contributed equally to this work

[*]Corresponding author: Kisuk Kang (E-mail: matlgen1@snu.ac.kr)

This supplementary information file includes:

Notes S1–S2

Figures S1–S16

References 1–2

Supplementary Notes

Supplementary Note 1. To establish a regression equation that accurately describes the site energy of lithium ions, we quantified the environmental factors surrounding the lithium ions that could influence the site energy of lithium ions and presented a total of 10 factors as descriptors. The distortion index values for lithium octahedron were calculated using the following equation:[1]

$$Distortion\ index = \frac{1}{n}\sum_{i=1}^{n}\frac{|l_i - l_{aver}|}{l_{aver}}$$

Where l_i denotes the bond length between lithium ion and the ith oxygen atom and l_{aver} is the average bond length.

To quantitatively assess octahedral distortion independent of the polyhedron's effective size, the quadratic elongation is defined by the following equation:[2]

$$Quadratic\ elongation = \frac{1}{n}\sum_{i=1}^{n}\left(\frac{l_i}{l_0}\right)^2$$

Where l_0 represents the center-to-vertex distance of a regular octahedron with an equivalent volume. In addition to bond length, bond angle variance was considered to account for the distortion of the octahedron caused by deviations in bond angles. The Bond angle variance is calculated as the following equation:[2]

$$Bond\ angle\ variance = \frac{1}{m-1}\sum_{i=1}^{m}(\emptyset_i - \emptyset_0)^2$$

Where m denotes the product of the number of faces in the polyhedron and 3/2, representing the total number of bond angles. $\emptyset_i$ signifies the ith bond angle, while $\emptyset_0$ represents the ideal bond angle for a regular polyhedron, such as 90 degrees for an octahedron.

Calculating the coordination number for a central atom in a coordination polyhedron presents challenges, particularly in cases of relatively distorted structures. However, the effective coordination number involves summing the contributions of surrounding atoms using a weighting scheme, where atoms are considered as fractional entities ranging from 0 to 1. As the distance from the central atom to a surrounding atom increases, their contribution approaches zero. The effective coordination number is defined as the sum of each quantity w_i which is called the bond weight of the ith bond. The bond weight is defined as the following equation:[2]

$$w_i = e^{\left[1-\left(\frac{l_i}{l_{aver}}\right)^6\right]} \text{ and } l_{aver} = \frac{\sum_i l_i e^{\left[1-\left(\frac{l_i}{l_{min}}\right)^6\right]}}{\sum_i e^{\left[1-\left(\frac{l_i}{l_{min}}\right)^6\right]}}$$

, where l_{min} is the shortest bond length in the coordination octahedron.

Supplementary Note 2. To elucidate the lithium diffusion mechanism from a local perspective by analyzing various structures that can appear in DRX, we introduced the model system which contains various types of 0-TM channel and defined the model system as 'diffusion cluster'. The diffusion cluster is an optimized model system for analyzing the one-step hopping event of lithium because it can consider factors that determine the characteristics of hopping such as site energy, high-order neighbor of lithium ion and activation barrier. It can also simulate realistic models as closely as possible by avoiding extreme compositions, such as the environment that 20 lithium ions are concentrated in a specific region, that cannot be realized. Furthermore, unit cell size is large enough to avoid introducing artificial correlated motion due to periodic boundary conditions and the unit cell configuration is verified in Supplementary Figs. S10. The diffusion cluster consists of 20 cations, while the unit cell, which encompasses the diffusion cluster, comprises 32 cations. According to the composition ratio of $Li_{1.2}Mn_{0.4}Ti_{0.4}O_2$, the 20 cations in the diffusion cluster is composed of 12 lithium ions, 4 manganese ions, and 4 titanium ions. The unit cell, which contains the diffusion cluster and is composed of 32 cations, includes 19 lithium ions, 7 manganese ions, and 6 titanium ions. Each cation maintains a fixed valence state of Li^{1+}, Mn^{3+}, and Ti^{4+} to match the composition ratio accurately. To incorporate partial ordering within $Li_{1.2}Mn_{0.4}Ti_{0.4}O_2$, we fixed lithium ions at cation sites with spinel-like ordering[3] within the diffusion cluster and determined the positions of the remaining cations through enumeration.

Supplementary Figures

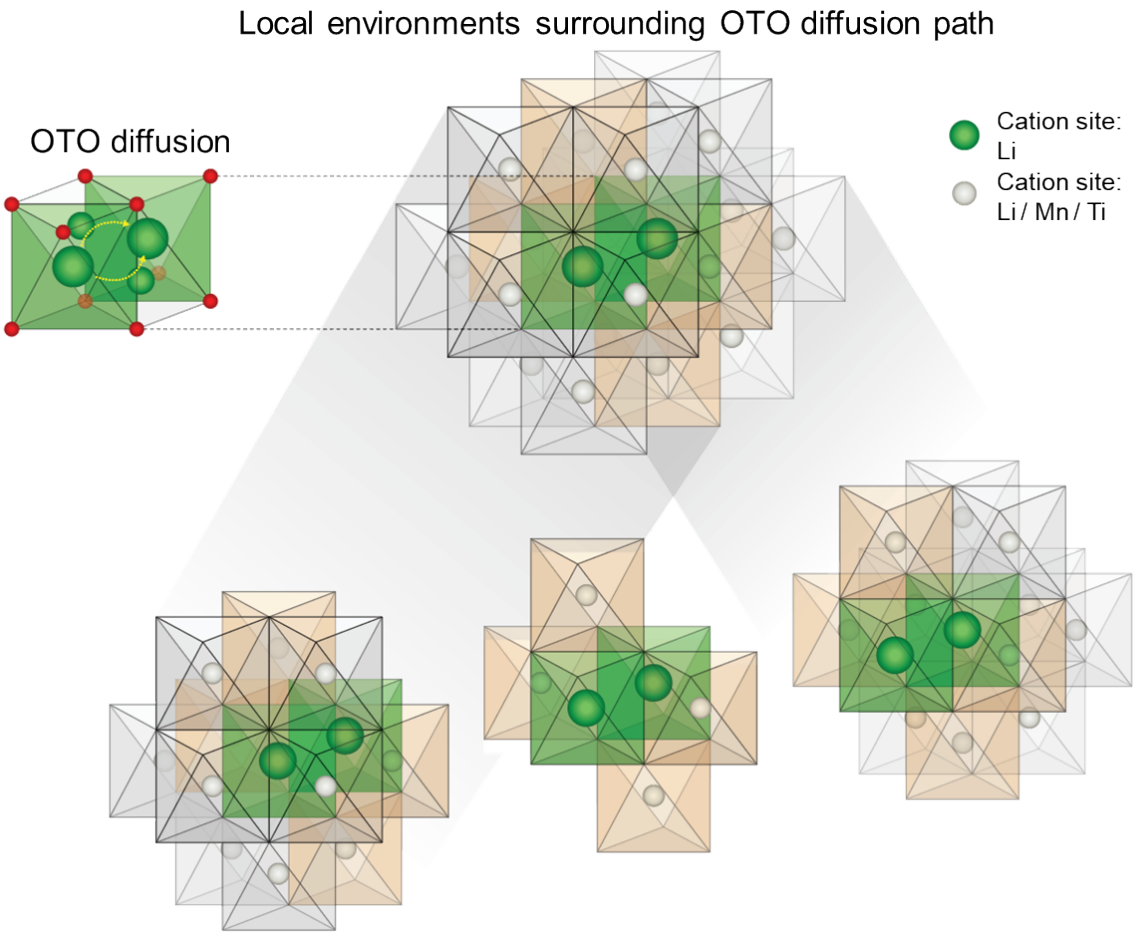

Fig. S1. Components of diffusion cluster. These clusters comprise 12 nearest neighboring octahedral sites (gray) affecting the lithium octahedral site energy and another set of 12 nearest neighboring octahedral sites affecting the adjacent lithium octahedral site. Notably, four octahedral sites (orange) overlap between these two sets, exerting considerable influence on the site energy of the intermediate state during lithium ion hopping.

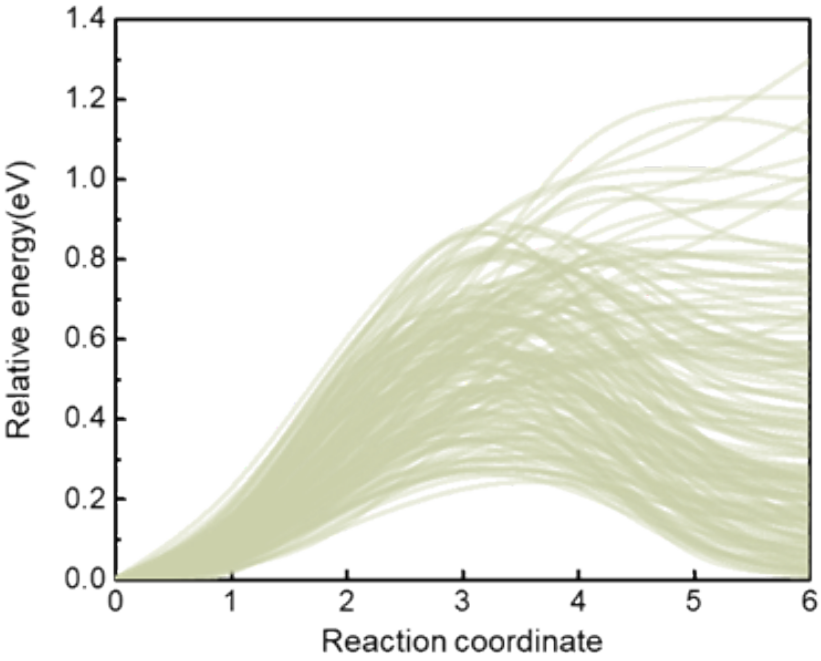

Fig. S2. Minimum energy paths during one hopping event of lithium ion in DRX obtained from NEB calculations. Various configurations of energy profiles show large distribution of the activation barrier and site energy difference as high as 1.3 eV.

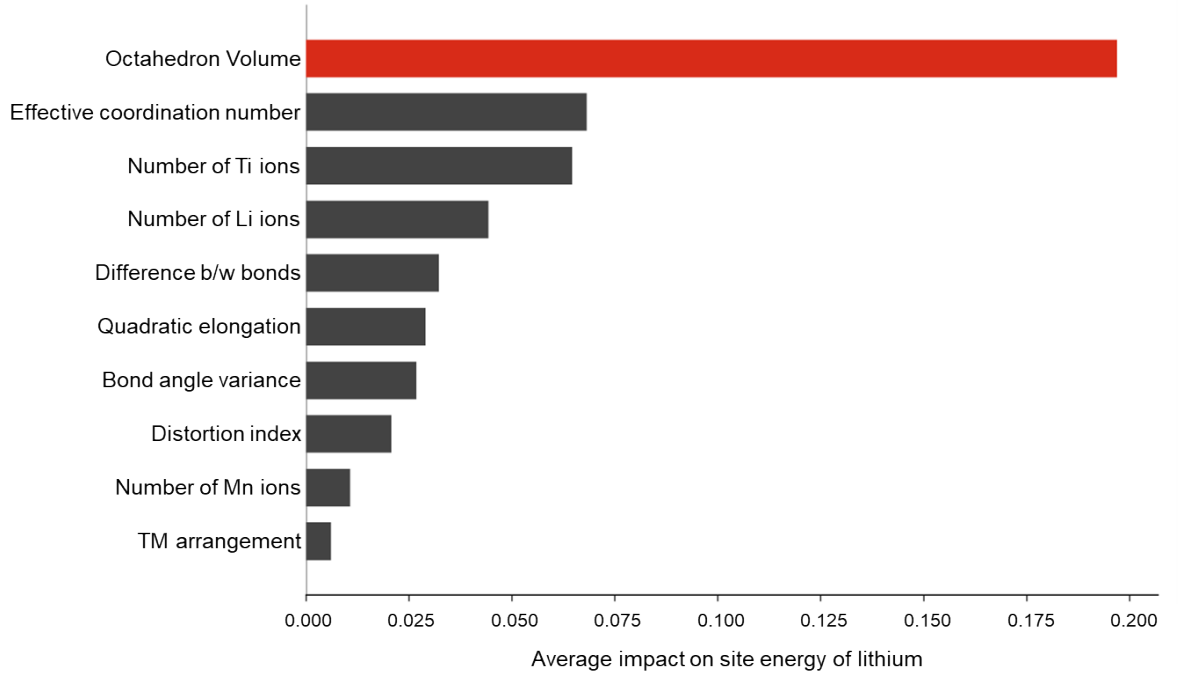

Fig. S3. Factors were ranked based on their respective impacts on the lithium site energy in $Li_{1.2}Mn_{0.4}Ti_{0.4}O_2$ obtained from SHAP values. The volume of the lithium octahedron exerts the most significant influence on site energy of lithium.

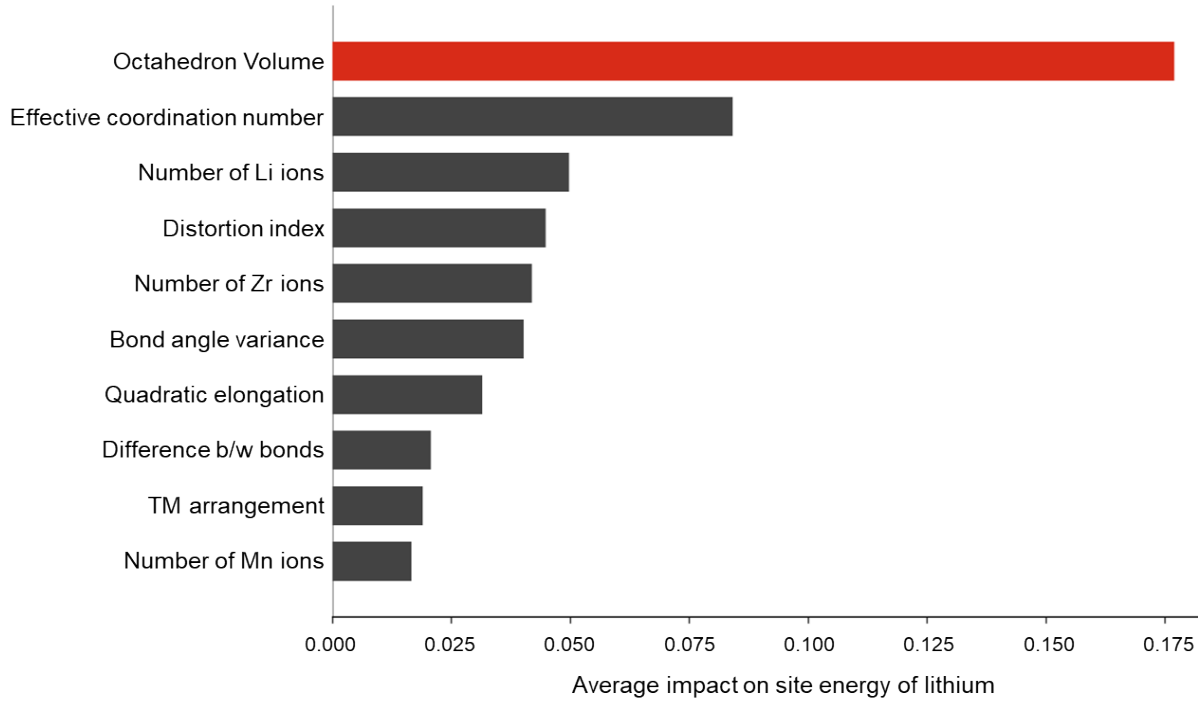

Fig. S4. Factors were ranked based on their respective impacts on the lithium site energy in $Li_{1.2}Mn_{0.4}Zr_{0.4}O_2$ obtained from SHAP values. The volume of the lithium octahedron exerts the most significant influence on site energy of lithium.

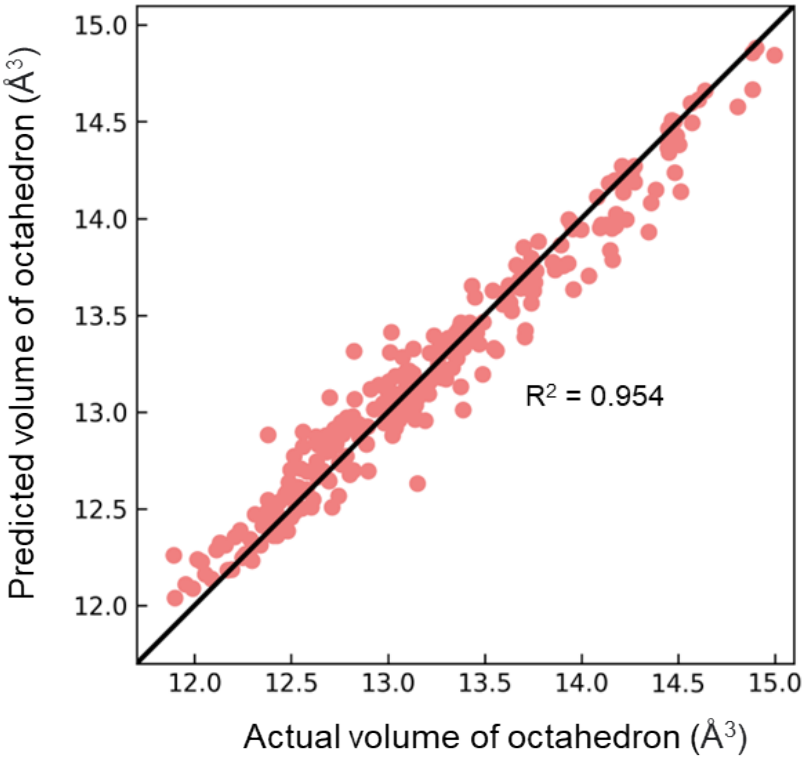

Fig. S5. Regression performance of XGBoost predicting volume of lithium octahedron in $Li_{1.2}Mn_{0.4}Ti_{0.4}O_2$. The octahedron volume regression using machine learning achieved around 0.95 R-squared values for $Li_{1.2}Mn_{0.4}Ti_{0.4}O_2$, indicating the feasibility of the model.

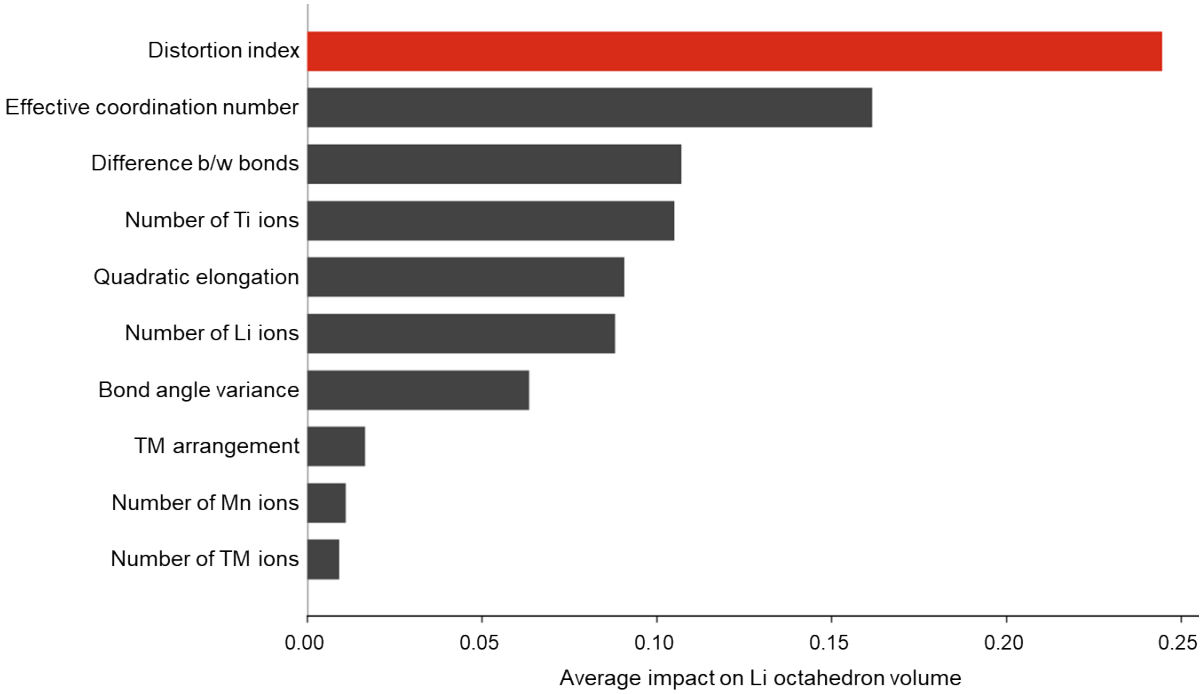

Fig. S6. Factors were ranked based on their respective impacts on the volume of lithium octahedron in $Li_{1.2}Mn_{0.4}Ti_{0.4}O_2$ obtained from SHAP values. The distortion index exerts the most significant influence on the volume of lithium octahedron.

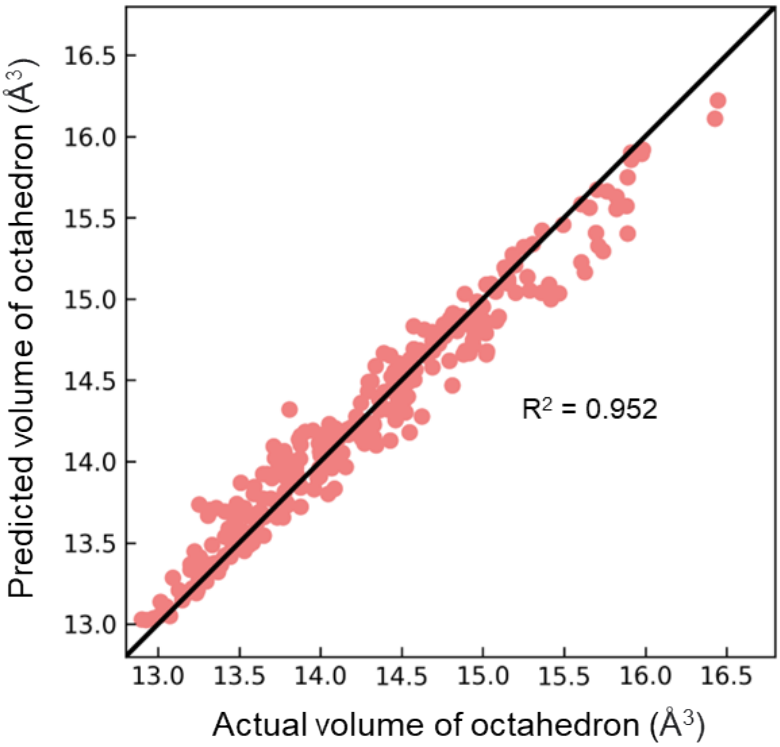

Fig. S7. Regression performance of XGBoost predicting volume of lithium octahedron in $Li_{1.2}Mn_{0.4}Zr_{0.4}O_2$. The octahedron volume regression using machine learning achieved around 0.95 R-squared values for $Li_{1.2}Mn_{0.4}Zr_{0.4}O_2$, indicating the feasibility of the model.

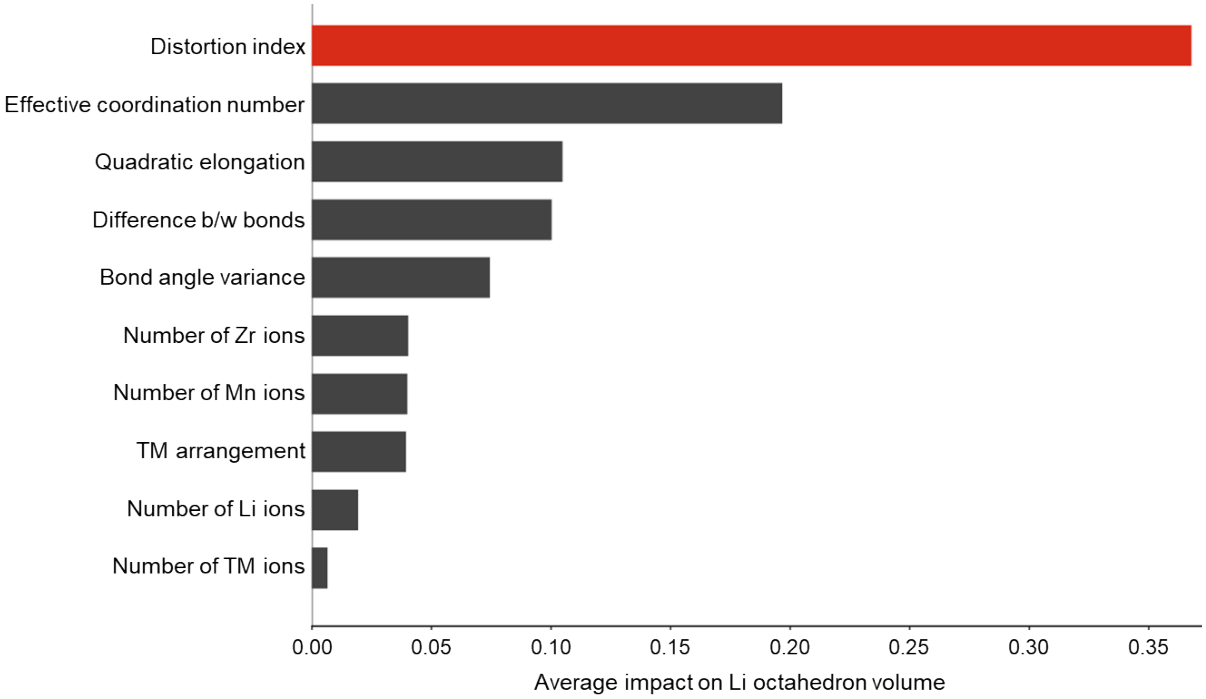

Fig. S8. Factors were ranked based on their respective impacts on the volume of lithium octahedron in $Li_{1.2}Mn_{0.4}Zr_{0.4}O_2$ obtained from SHAP values. The distortion index exerts the most significant influence on the volume of lithium octahedron.

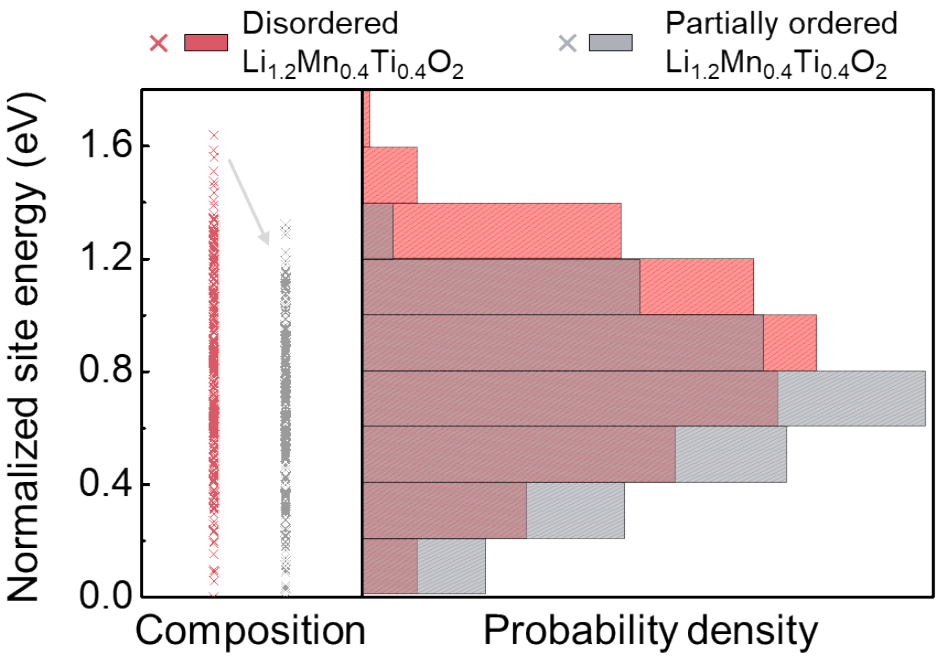

Fig. S9. The site energy calculations for $Li_{1.2}Mn_{0.4}Ti_{0.4}O_2$ and $Li_{1.2}Mn_{0.4}Ti_{0.4}O_2$ with partial ordering. It reveals that the site energy distribution was decreased by introducing partial ordering of cations.

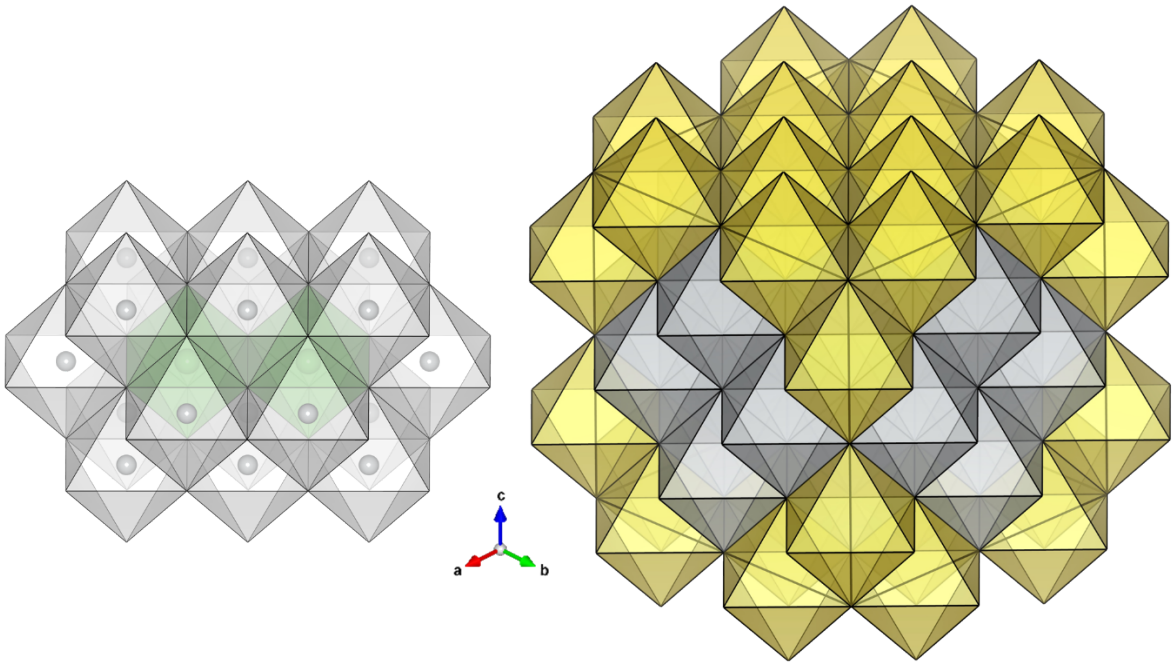

Fig. S10. The diffusion cluster observed from different perspective (left) and the unit cell containing the diffusion cluster (right). The gray octahedra represent the sites of cations that form the diffusion cluster, while the yellow octahedra represent the sites of cations that constitute the surrounding unit cell. The unit cell consists of a total of 32 cations.

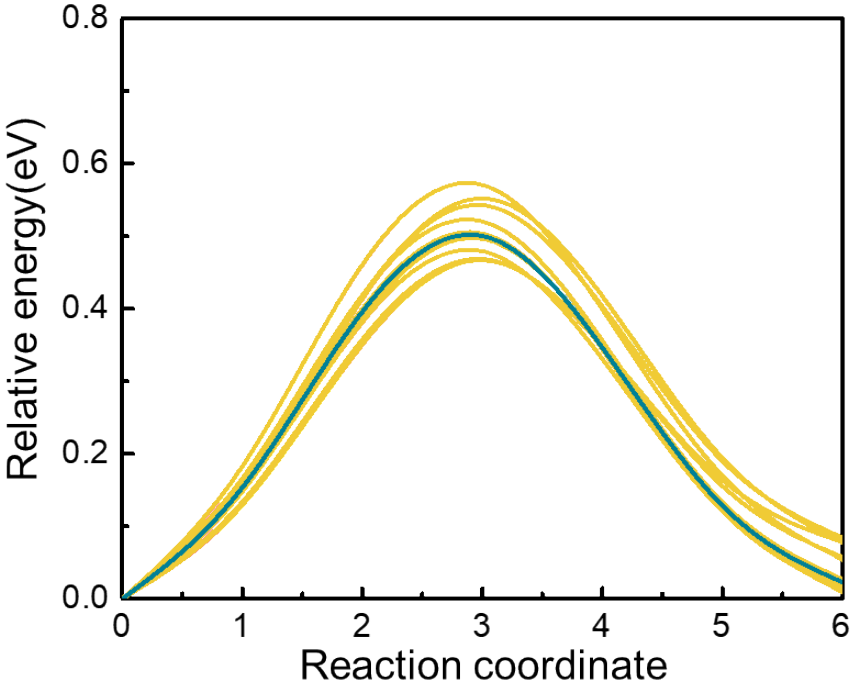

Fig. S11. The minimum energy paths of lithium diffusion within the same diffusion cluster but in different unit cells. The blue minimum energy path serves as a reference, while the yellow minimum energy paths are obtained from unit cells where the diffusion cluster is fixed, but the arrangement of remaining cations within the unit cell is varied. The cations outside the diffusion cluster have negligible impact on the lithium hopping within the diffusion cluster.

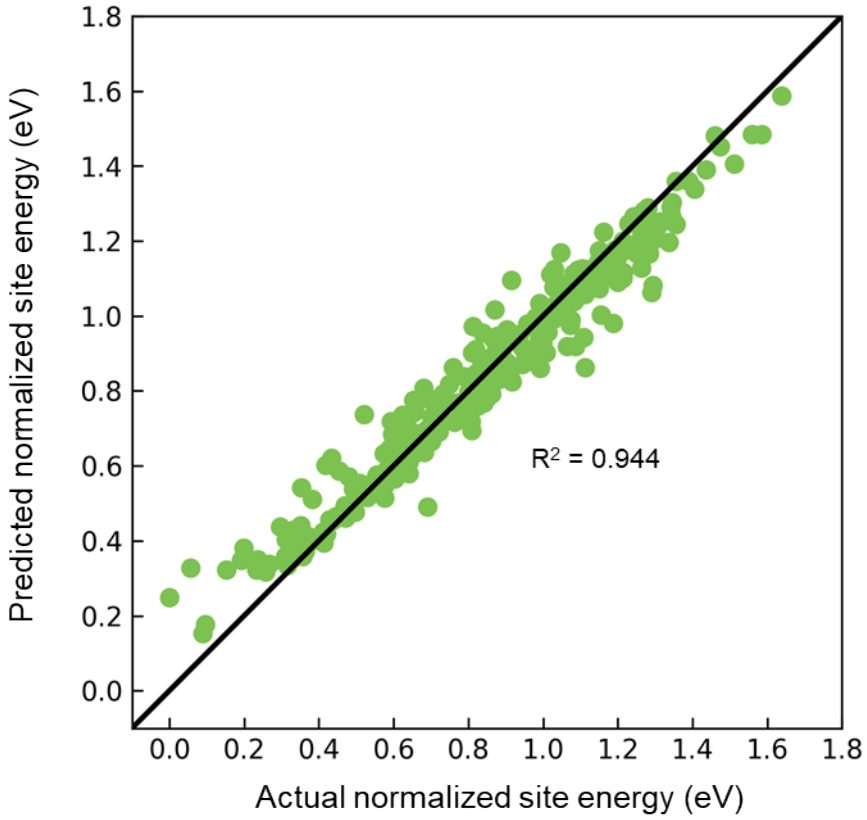

Fig. S12. Regression performance of XGBoost predicting lithium site energy in $Li_{1.2}Mn_{0.4}Ti_{0.4}O_2$. The site energy regression using machine learning achieved around 0.95 R-squared values for $Li_{1.2}Mn_{0.4}Ti_{0.4}O_2$, indicating the feasibility of the model.

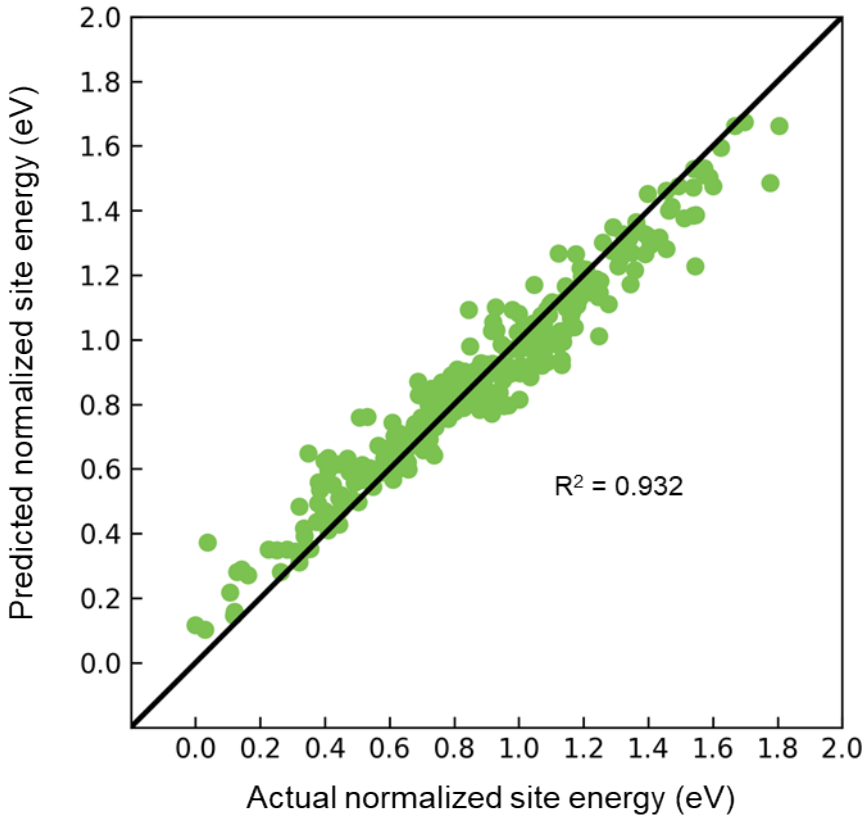

Fig. S13. Regression performance of XGBoost predicting lithium site energy in $Li_{1.2}Mn_{0.4}Zr_{0.4}O_2$. The site energy regression using machine learning achieved around 0.95 R-squared values for $Li_{1.2}Mn_{0.4}Zr_{0.4}O_2$, indicating the feasibility of the model.

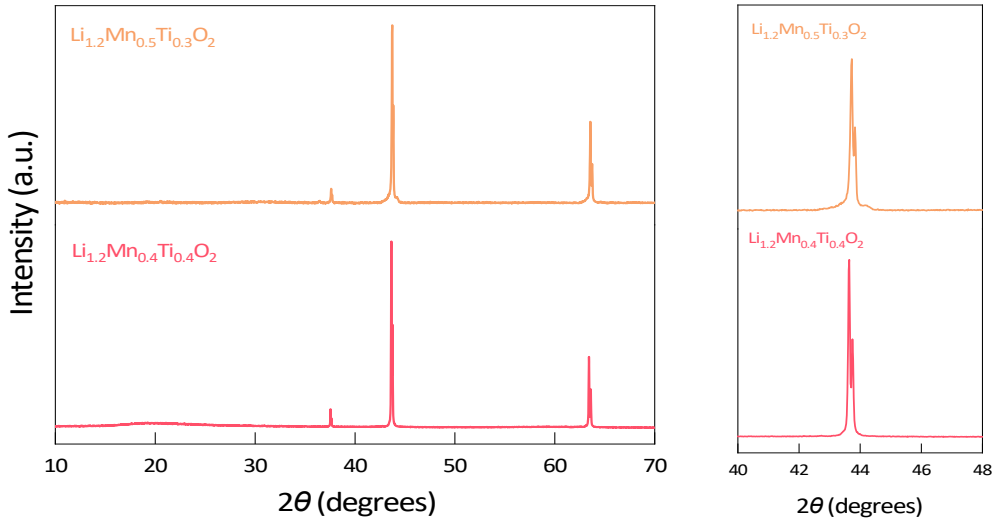

Fig. S14. X-ray diffraction patterns of as-synthesized $Li_{1.2}Mn_{0.4}Ti_{0.4}O_2$ and $Li_{1.2}Mn_{0.5}Ti_{0.3}O_2$. Right-shifting of the peaks in $Li_{1.2}Mn_{0.5}Ti_{0.3}O_2$ with respect to $Li_{1.2}Mn_{0.4}Ti_{0.4}O_2$ reveals that the lattice parameter decreases with substitution of Ti^{4+} (0.61 Å) to Mn^{4+} (0.53 Å).

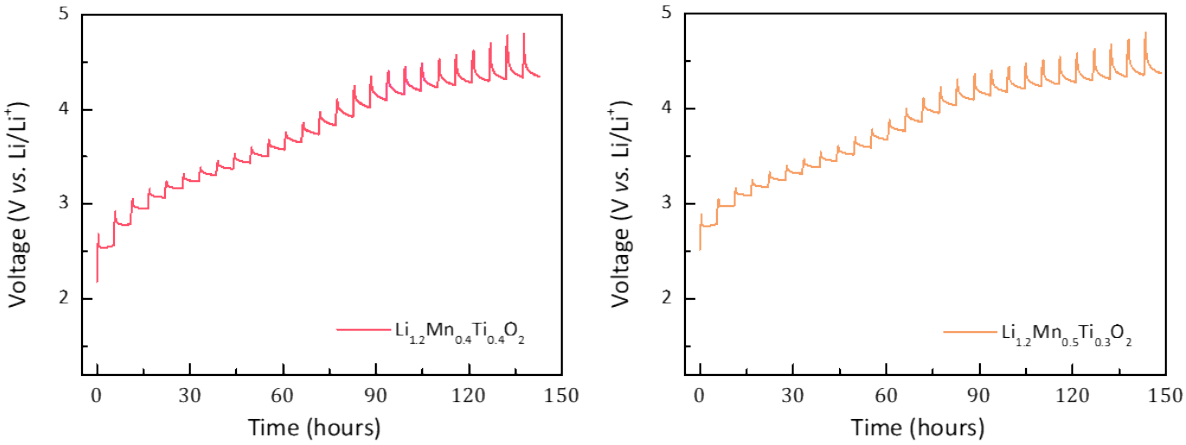

Fig. S15. The galvanostatic intermittent titration technique (GITT) profile of $Li_{1.2}Mn_{0.4}Ti_{0.4}O_2$ (left) and $Li_{1.2}Mn_{0.5}Ti_{0.3}O_2$ (right).

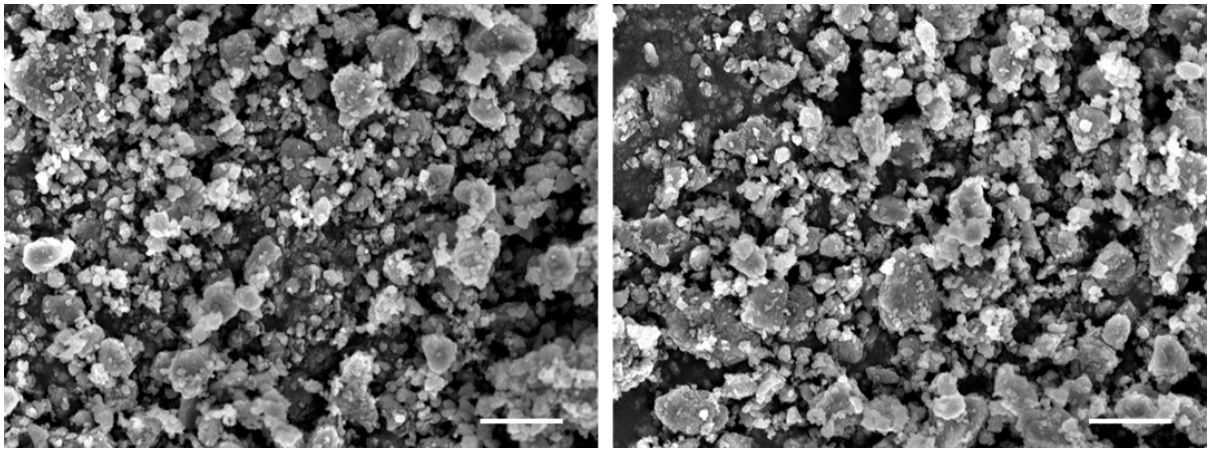

Fig. S16. SEM images (scale bars, 1 μm) of ball-milled $Li_{1.2}Mn_{0.4}Ti_{0.4}O_2$ (left) and $Li_{1.2}Mn_{0.5}Ti_{0.3}O_2$ (right) with similar particle sizes of ~200 nm. The relatively small 10 nm-scale particles are Super P, the carbon mixed during pulverization, while the relatively large 100 nm-scale particles are DRX cathode active materials.

References

[1] W. H. Baur, E. Tillmanns, *Acta Crystallographica Section B: Structural Science* **1986**, *42*, 95-111.

[2] K. Robinson, G. Gibbs, P. Ribbe, *Science* **1971**, *172*, 567-570.

[3] A. Urban, J. Lee, G. Ceder, *Advanced Energy Materials* **2014**, *4*, 1400478.